AGU PUBLICATIONS

Geophysical Research Letters

RESEARCH LETTER
10.1002/2017GL073859

Key Points:
- We detect significant HCHO trends over North America from space
- We see evidence of changing emissions of VOCs from space, in particular from oil/gas operations
- The impact of declining NO_x emissions on HCHO columns is greatest in the southeastern U.S.

Supporting Information:
- Supporting Information S1

Correspondence to:
L. Zhu,
leizhu@fas.harvard.edu

Citation:
Zhu, L., L. J. Mickley, D. J. Jacob, E. A. Marais, J. Sheng, L. Hu, G. G. Abad, and K. Chance (2017), Long-term (2005–2014) trends in formaldehyde (HCHO) columns across North America as seen by the OMI satellite instrument: Evidence of changing emissions of volatile organic compounds, *Geophys. Res. Lett.*, *44*, doi:10.1002/2017GL073859.

Received 19 APR 2017
Accepted 17 JUN 2017
Accepted article online 20 JUN 2017

Long-term (2005–2014) trends in formaldehyde (HCHO) columns across North America as seen by the OMI satellite instrument: Evidence of changing emissions of volatile organic compounds

Lei Zhu[1], Loretta J. Mickley[1], Daniel J. Jacob[1,2], Eloïse A. Marais[1,3], Jianxiong Sheng[1], Lu Hu[1,4], Gonzalo González Abad[5], and Kelly Chance[5]

[1]John A. Paulson School of Engineering and Applied Sciences, Harvard University, Cambridge, Massachusetts, USA, [2]Department of Earth and Planetary Sciences, Harvard University, Cambridge, Massachusetts, USA, [3]Now at School of Geography, Earth and Environmental Sciences, University of Birmingham, Edgbaston, UK, [4]Now at Department of Chemistry and Biochemistry, University of Montana, Missoula, Montana, USA, [5]Harvard-Smithsonian Center for Astrophysics, Cambridge, Massachusetts, USA

Abstract Satellite observations of formaldehyde (HCHO) columns provide top-down information on emissions of highly reactive volatile organic compounds (VOCs). We examine the long-term trends in HCHO columns observed by the Ozone Monitoring Instrument from 2005 to 2014 across North America. Biogenic isoprene is the dominant source of HCHO, and its emission has a large temperature dependence. After correcting for this dependence, we find a general pattern of increases in much of North America but decreases in the southeastern U.S. Over the Houston-Galveston-Brazoria industrial area, HCHO columns decreased by 2.2% a^{-1} from 2005 to 2014, consistent with trends in emissions of anthropogenic VOCs. Over the Cold Lake Oil Sands in the southern Alberta in Canada, HCHO columns increased by 3.8% a^{-1}, consistent with the increase in crude oil production there. HCHO variability in the northwestern U.S. and Midwest could be related to afforestation and corn silage production. Although NO_x levels can affect the HCHO yield from isoprene oxidation, we find that decreases in anthropogenic NO_x emissions made only a small contribution to the observed HCHO trends.

Plain Language Summary We use satellite observations to diagnose long-term trends in HCHO columns across North America from 2005 to 2014. HCHO generally increased from 2005–2009 to 2010–2014 but decreased in the southeastern U.S. We find significant regional trends in excess of 20% related to decreases in urban anthropogenic VOC emissions (Houston metropolitan area) and increases in oil/gas production (oil sands in western Canada). Significant regional trends in the northwestern U.S. and in the Midwest may be driven by afforestation and agricultural activity. The impact of declining NO_x emission over the U.S. on HCHO columns is likely small over this time frame.

1. Introduction

Formaldehyde (HCHO), a high-yield product from the atmospheric oxidation of volatile organic compounds (VOCs), is detectable from space as a total column by solar UV backscatter [*Chance et al.*, 2000]. Remotely sensed HCHO columns have been used as a proxy to constrain underlying VOC emissions from biogenic sources [*Palmer et al.*, 2003; *Millet et al.*, 2008; *Stavrakou et al.*, 2009; *Marais et al.*, 2012; *Barkley et al.*, 2013; *Bauwens et al.*, 2016], anthropogenic sources [*Fu et al.*, 2007; *Marais et al.*, 2014; *Zhu et al.*, 2014; *Souri et al.*, 2017], and open fires [*Shim et al.*, 2005; *Gonzi et al.*, 2011]. Here we use a 10 year record (2005–2014) of HCHO columns from the Ozone Monitoring Instrument (OMI) to infer long-term HCHO trends over North America and relate them to changes in anthropogenic emissions, oil/gas operations, land cover, and agriculture.

Most of the HCHO column over North America during the growing season is from biogenic isoprene [*Palmer et al.*, 2003; *Millet et al.*, 2006, 2008; *Bauwens et al.*, 2016]. Anthropogenic enhancements in urban/industrial plumes are detectable on top of this biogenic background [*Boeke et al.*, 2011; *Zhu et al.*, 2014, 2017]. Outside of the growing season HCHO is undetectable [*Abbot et al.*, 2003], which reflects both the lack of isoprene and the slower rate of VOC photochemical oxidation under weaker solar radiation [*Zhu et al.*, 2014].

The record of HCHO column observations from space began with the Global Ozone Monitoring Experiment (GOME) instrument launched in 1995 [*Chance et al.*, 2000]. *De Smedt et al.* [2010, 2015] analyzed long-term trends in HCHO column data from GOME and successor satellite instruments (Scanning Imaging Absorption Spectrometer for Atmospheric Chartography , GOME-2, and OMI) to infer -3.5% a^{-1} to $+4.3\%$ a^{-1} trends over 1997–2009 in several U.S. cities, and more recent 2004–2014 decreases over the northern and eastern U.S. including Pennsylvania (-2.1% a^{-1}), Houston (-1.1% a^{-1}), and California (-0.2% a^{-1}). Here we use the consistent high-resolution record available from OMI for an analysis of trends across North America over the 2005–2014 period, building on our recent validation of the OMI data with aircraft observations [*Zhu et al.*, 2016], and correcting for the temperature dependence of isoprene emission that is known to drive HCHO variability on a month-to-month basis [*Palmer et al.*, 2006; *Duncan et al.*, 2009].

2. OMI HCHO Column Data and Temperature Correction

OMI is a UV/Vis nadir solar backscatter spectrometer launched in 2004 on the Aura satellite in a polar Sun-synchronous orbit [*Levelt et al.*, 2006]. It observes the whole globe daily at 13:30 local time with a spatial resolution of 13×24 km^2 (nadir) to ~25×105 km^2 (outermost swath-angle) [*Levelt et al.*, 2006; *de Graaf et al.*, 2016]. We use OMI HCHO Version 2.0 (Collection 3) retrieval [*González Abad et al.*, 2015] from the Smithsonian Astrophysical Observatory (OMI-SAO). The retrieval includes application of a "reference sector correction" to distinguish the HCHO enhancement over background values [*Khokhar et al.*, 2005; *Zhu et al.*, 2016]. The single-scene precision of the retrieval is 1×10^{16} molecules cm^{-2} (absolute) from spectral fitting and 45–105% (relative) from the air mass factor (AMF) [*González Abad et al.*, 2015]. The spectral fitting error is random while the AMF error has both random and systematic components. The precision can be improved by spatial and temporal averaging [*De Smedt et al.*, 2008; *Boeke et al.*, 2011; *Zhu et al.*, 2016].

Zhu et al. [2016] validated the OMI-SAO HCHO columns with high-quality aircraft measurements from the Studies of Emissions and Atmospheric Composition, Clouds and Climate Coupling by Regional Surveys flight campaign over the southeastern U.S. in August–September 2013 [*Toon et al.*, 2016]. The OMI-SAO data showed strong spatial correlation with the aircraft and day-to-day temporal variability consistent with that expected from isoprene emission. The data were biased low by 37% relative to the aircraft, and here we apply a uniform and constant correction factor of 1.6 to account for this. Because the correction factor is uniform and constant, it has no effect on our results of relative trends in HCHO columns. Other OMI-SAO validation studies using aircraft data are consistent with this correction [*González Abad et al.*, 2014; *Anderson et al.*, 2016]. We restrict our analysis to May–September when the HCHO data over source regions are generally well above the detection limit. We select only those data that (1) pass all fitting and statistical quality checks (MainDataQualityFlag = 0), (2) have cloud fraction less than 0.3 and solar zenith angle less than 60°, (3) are from rows 1–20 and 55–60 of the OMI detector, and (4) have a vertical column density within the range of -0.5×10^{16} molecules cm^{-2} to 10×10^{16} molecules cm^{-2}. The third criterion excludes data points affected by the growing problem of OMI "row anomalies" (http://projects.knmi.nl/omi/research/product/rowanomaly-background). The fourth criterion removes 5.8% of the data as outliers.

OMI-SAO HCHO columns show significant drift caused by instrument aging [*Marais et al.*, 2012; *Zhu et al.*, 2014]. We correct for the drift by temporal linear regression of the deseasonalized zonal mean monthly averaged HCHO columns for 2005–2014 in 0.5° latitudinal increments over the remote Pacific (160°–140°W, 20°–60°N), where no trend in HCHO is expected. The drift varies from 3.8×10^{13} molecules cm^{-2} a^{-1} at 30°N to 1.4×10^{14} molecules cm^{-2} a^{-1} at 60°N.

Temperature drives most of the interannual variability of HCHO columns over North America, reflecting the doubling of isoprene emissions for about every 7 K temperature increase [*Guenther et al.*, 2006; *Palmer et al.*, 2006; *Duncan et al.*, 2009]. Accounting for this dependence is important in trend analyses. We compute the temperature-independent changes in HCHO columns from 2005 to 2014 as follows. We first assign a temperature to each satellite pixel based on its location and passing time, using the hourly surface skin temperature data (0.5° × 0.667°) from the Modern-Era Retrospective Analysis for Research and Applications, version 2 (MERRA-2; https://gmao.gsfc.nasa.gov/reanalysis/MERRA). We then allocate the satellite pixels into 120 temperature bins in increments of 0.25 K over the range of 288 K to 318 K. We also tried 0.5 K as the temperature increment and found that leads to less uniformity in the spatial patterns of HCHO change. For each temperature bin *i*, we divide the array of satellite pixels into two periods, 2005–2009 and

2010–2014, denoted as periods 1 and 2. We then follow the averaging method of *Zhu et al.* [2017] to map the HCHO column amounts for the two periods onto a 0.5° × 0.5° horizontal grid, with $N_{i,j,1}$ and $N_{i,j,2}$ overlapping pixels collected in each gridcell j for the two periods. The change in mean HCHO column from 2005–2009 to 2010–2014 for temperature increment i in gridcell j is calculated as

$$\Delta\bar{\Omega}_{i,j} = \bar{\Omega}_{i,j,2} - \bar{\Omega}_{i,j,1} \tag{1}$$

where $\bar{\Omega}_{i,j,1}$ and $\bar{\Omega}_{i,j,2}$ represent the mean HCHO column amounts for each period. We compute the temperature-independent change in column HCHO for gridcell j as the mean of the changes across all the temperature bins with at least 25 measurements for each period, weighted by the sum of pixels in each bin:

$$\Delta\bar{\Omega}_j = \frac{\sum_i \Delta\bar{\Omega}_{i,j} N_{i,j}}{\sum_i N_{i,j}} \tag{2}$$

$$N_{i,j} = N_{i,j,1} + N_{i,j,2} \tag{3}$$

To increase confidence in our analysis, we consider only those gridcells with valid changes in at least 20 temperature bins. Each $\Delta\bar{\Omega}_j$ has contributions from at least 1000 satellite pixels. We use the t test ($p < 0.05$) to test for significance of nonzero $\Delta\bar{\Omega}_j$.

3. Results and Discussion

Figure 1 shows the 2005–2014 mean May–September HCHO columns. High values in the southeastern U.S. are from isoprene oxidation [*Palmer et al.*, 2003; *Millet et al.*, 2008; *Zhu et al.*, 2016]. Hot spots in the west are mainly from fires [*Zhu et al.*, 2017]. Also shown in Figure 1 are the absolute and relative temperature-independent changes in HCHO columns from 2005–2009 (period 1) to 2010–2014 (period 2). Figure S1 in the supporting information shows trends without correcting for temperature.

De Smedt et al. [2015] previously showed a HCHO column decrease over the southeastern U.S. at a rate of 0.1–0.3 × 10^{15} molecules cm^{-2} a^{-1} from 2004 to 2014 based on an independent OMI retrieval product. This is equivalent to a net decrease of 0.5–1.5 × 10^{15} molecules cm^{-2} from periods 1 to 2, consistent with our results in Figure 1. In other areas, however, our study yields trends different in sign from those in *De Smedt et al.* [2015]. For example, we find prevailing positive trends over central and northwestern North America, but *De Smedt et al.* [2015] reported generally negative trends for those areas. Reasons for this discrepancy are unclear but may reflect differences in the HCHO retrievals [*Zhu et al.*, 2016] and/or the time periods studied. *De Smedt et al.* [2015] did not provide detailed attribution of their reported trends. Here we attempt to attribute the HCHO trends diagnosed in our study to various potential factors.

We focus our analysis on clusters of gridcells with significant HCHO change, enclosed by circles in Figure 1. The four clusters, their 2005–2009 to 2010–2014 changes, and the 95% confidence intervals for these changes are (a) the Houston-Galveston-Brazoria area (HGB; −14.6 ± 5.3%), (b) the Cold Lake Oil Sands in the southern Alberta (37.2 ± 15.4%), (c) the northwestern U.S. (25.4 ± 11.6%), and (d) Illinois and Missouri (19.0 ± 9.4%). These regions were not examined in *De Smedt et al.* [2015], except for HGB.

Figure 1 gives only the mean changes across the two periods. To identify the potential explanatory variables driving these mean changes, we construct time series of monthly mean HCHO columns spatially averaged over the regions enclosed by circles in Figure 1. In this spatial averaging, we consider only those gridcells where the HCHO change between the two time periods is statistically significant (Figure 1, bottom). We then calculate the temporal correlation between these HCHO time series and those of the potential explanatory variables. To remove the temperature effect on the HCHO time series, we determine for each gridcell the local exponential dependence of the monthly mean HCHO column on monthly mean surface temperature [*Palmer et al.*, 2006; *Duncan et al.*, 2009; *Zhu et al.*, 2014] and normalize the observed HCHO columns to the mean May–September 2005–2014 temperature for that gridcell. We report only statistically significant trends using the generalized Deming regression [*Cornbleet and Gochman*, 1979], with $p < 0.05$ as the threshold for significance unless otherwise specified.

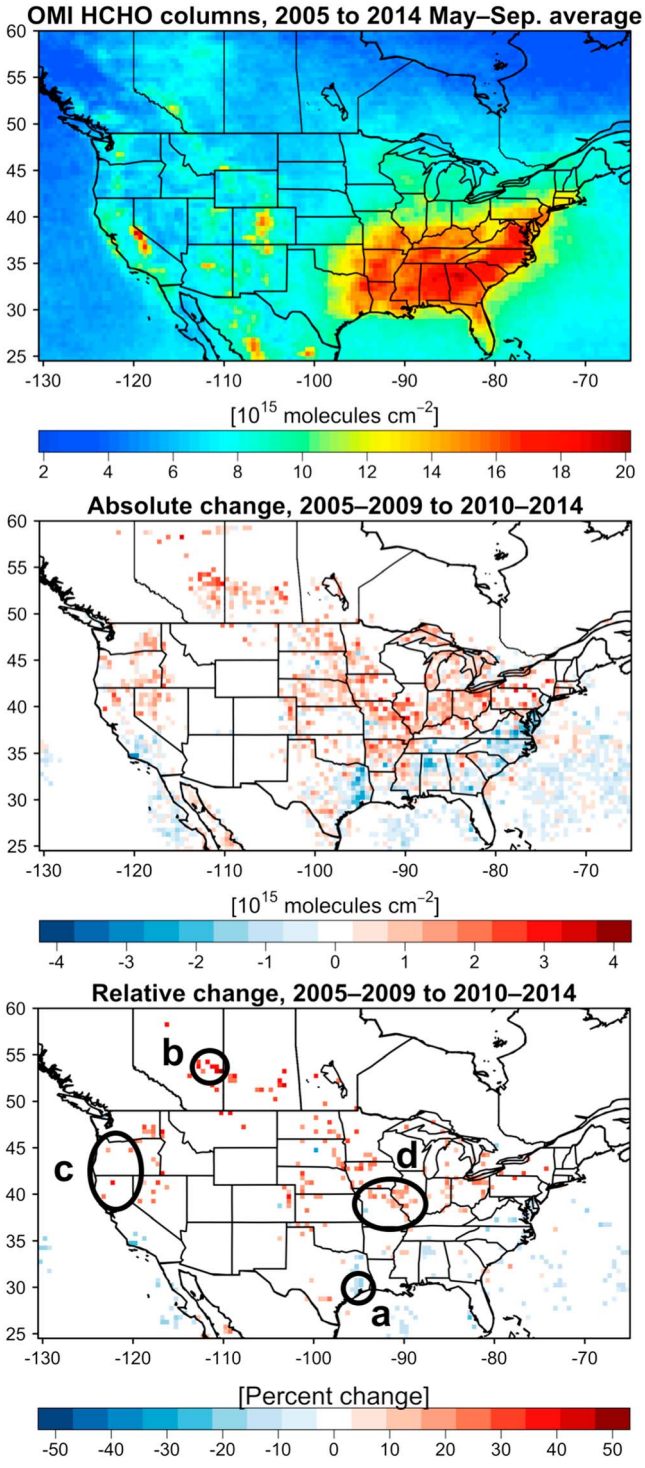

Figure 1. (top) Mean 2005–2014 HCHO columns for May–September over the U.S. and southern Canada and trends from 2005–2009 to 2010–2014, (middle) absolute trends and (bottom) relative trends. Figure 1 (bottom) shows only statistically significant ($p < 0.05$) relative changes. The circled regions represent areas discussed in the text: (a) Houston-Galveston-Brazoria (HGB) in Texas; (b) Cold Lake Oil Sands in Alberta, Canada; (c) northwestern U.S.; and (d) Illinois and Missouri.

Figure 2 shows the 2005–2014 time series of mean May–September temperature-corrected HCHO columns in the four regions, together with time series of hypothesized explanatory variables. We report latitude and longitude coordinates for grid-cells in those regions in Table S2 in the supporting information. In HGB, HCHO columns decline by $-2.2 \pm 1.1\%\ a^{-1}$ in a trend that strongly correlates with a concurrent decrease in anthropogenic point source VOC emissions of $-5.2 \pm 0.6\%\ a^{-1}$ (https://www.tceq.texas.gov/airquality/airsuccess/airSuccessEmissions). The HCHO trend is also consistent with measurements from the TexAQS aircraft campaigns in 1999 and 2006, which reveal decreases in median concentrations of 56% for ethene and 51% for propene over HGB between those two years [*Gilman et al.*, 2009]. *Zhu et al.* [2014] previously identified the HGB as the area in the U.S. where HCHO columns show the largest enhancement from anthropogenic highly reactive VOCs (mainly alkenes from point sources). The large isoprene-driven background in this region explains why the relative trends in HCHO columns are weaker than those in anthropogenic VOCs. The HGB results illustrate how remotely sensed HCHO can be used to detect trends in anthropogenic VOC emissions in areas where these are particularly high. *De Smedt et al.* [2015] reported a smaller trend of $-1.1 \pm 0.5\%\ a^{-1}$ in HCHO columns over the area of 100 km around Houston.

Over the Cold Lake Oil Sands in the southern Alberta, HCHO columns increase by $3.8 \pm 2.2\%\ a^{-1}$ over the 2005–2014 time period (Figure 2), concurrent with an increase in crude oil production in the same region ($4.8 \pm 0.7\%\ a^{-1}$) [*ETS, Energy Technical Services*, 2016]. Oil/gas operations can result in elevated HCHO levels through (1) primary emissions at sites where HCHO is used to scavenge H_2S from the gas

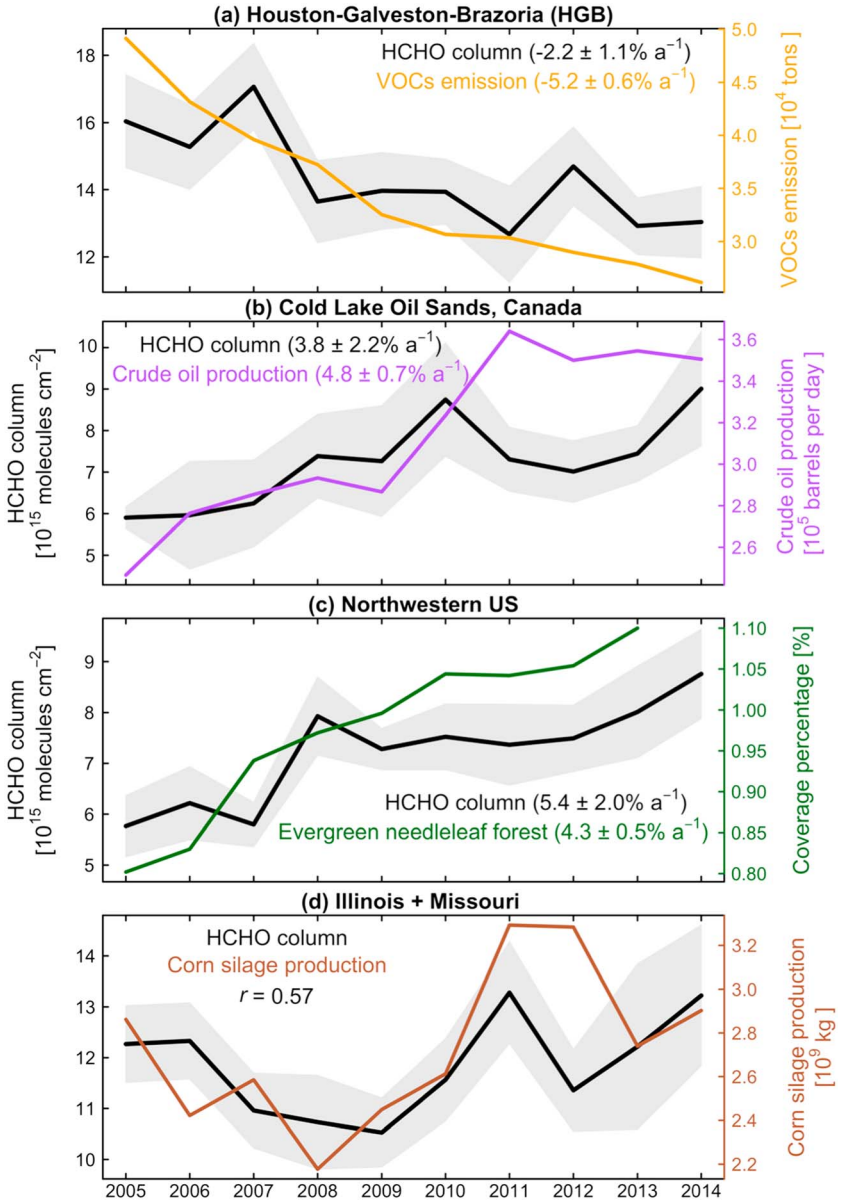

Figure 2. Time series of temperature-corrected May–September HCHO columns (black) and the potential explanatory variables driving HCHO variability (colors) from 2005 to 2014 in the four regions circled in Figure 1. Observed monthly mean HCHO columns are normalized to the 2005–2014 May–September mean temperature using the local dependence of HCHO on surface temperature. Shading represents one standard deviation across the monthly regional mean temperature-corrected HCHO columns. Explanatory variables depend on the region. The panels show (a) anthropogenic VOC emissions from point sources in the Houston-Galveston-Brazoria (HGB) area (https://www.tceq.texas.gov/airquality/airsuccess/airSuccessEmissions), (b) crude oil production in the Cold Lake Oil Sands [*ETS*, 2016], (c) mean coverage of evergreen needleleaf forests in the northwestern U.S. from MODIS MCD12Q1 land cover data [*Friedl et al.*, 2010], and (d) production of corn silage in Illinois and Missouri from the U.S. Department of Agriculture (http://quickstats.nass.usda.gov). Shown inset are the regression trends and corresponding 95% confidence intervals for regions with statistically significant trends ($p < 0.05$; Figures 2a–2c), as well as correlation coefficients between the temperature-corrected HCHO columns and the corn silage production (Figure 2d). For trend analysis, we use the generalized Deming regression [*Cornbleet and Gochman*, 1979] for HCHO columns, and the ordinary least squares regression for explanatory variables.

[*Amosa et al.*, 2010; *Kenreck*, 2014], (2) secondary formation from VOCs [*Gilman et al.*, 2013; *Edwards et al.*, 2014; *Macey et al.*, 2014], and (3) gas flaring [*Pikelnaya et al.*, 2013; *Marais et al.*, 2014]. *McLinden et al.* [2012] previously linked trends in bitumen production to the 2005–2011 increases in remotely sensed SO_2

and NO_2 columns over the Athabasca Oil Sands. Here we find that HCHO trends are mostly over the Cold Lake Oil Sands. Reasons for this spatial discrepancy are unclear.

Change in HCHO columns over the Floyd shale in northern Alabama in Figure 1 ($-1.0 \pm 2.2\%\ a^{-1}$) may be traced to declining gas production over the same time frame ($-4.4 \pm 0.4\%\ a^{-1}$; https://www.eia.gov/dnav/ng/hist/n9050al2a.htm). However, we find no HCHO enhancements nor trends in other oil/gas production regions (e.g., Pennsylvania, North Dakota, Oklahoma, and eastern Colorado), suggesting that HCHO emissions may depend on local practices.

In a few gridcells over the northwestern U.S., HCHO columns increase by $5.4 \pm 2.0\%\ a^{-1}$ (Figure 2), a trend highly correlated with increasing mean coverage of evergreen needleleaf forest cover across these gridcells. This coverage increased from 0.8% to 1.1% over the 2005–2013 period, or $4.3 \pm 0.5\%\ a^{-1}$. Evergreen needleleaf forests are an important source of isoprene [*Guenther et al.*, 2012] and thus of HCHO. The reforestation trend is likely part of the general trend of forest gains over the Pacific west, as reported by *Hansen et al.* [2013]. We were unable to link trends in HCHO columns elsewhere in North America to land cover trends. We do find a potential link between changing HCHO columns and land cover in Illinois and Missouri, where HCHO correlates moderately with corn silage production ($r = 0.57$; Figure 2). Silage, a fermented type of animal feed, emits an abundance of VOCs [*Hafner et al.*, 2013], some of which (e.g., aldehydes) could rapidly oxidize to form secondary HCHO. Primary HCHO may also be emitted directly from corn fields during harvesting [*Kaiser et al.*, 2015]. Elsewhere in the Corn Belt (e.g., Iowa, Nebraska, South Dakota, and North Dakota), however, we fail to find significant correlation between HCHO columns and production of either corn silage or grain, even in areas that show significant increases in HCHO over time (Figure 1). These more widespread increases could be linked to fuel ethanol production, which greatly enhances regional HCHO [*de Gouw et al.*, 2015]. U.S. production of fuel ethanol ramped up by 270% from 2005 to 2014 (https://www.eia.gov/totalenergy/data/monthly/index.php#renewable), and most ethanol refineries are located in the Midwest [*de Gouw et al.*, 2015].

Open fires may also serve as source of HCHO through primary emission or oxidation of nonmethane VOCs in the plume [*Marais et al.*, 2012; *Barkley et al.*, 2013; *Alvarado et al.*, 2015]. For example, the decline in HCHO columns over southwestern California (Figure 1) may be traced to exceptionally high fire emissions in 2007. However, we fail to find significant correlation between the 2005–2014 time series of temperature-corrected HCHO columns and fire emissions anywhere in the western U.S., where wildfires are common, or in the Southeast, where agricultural fires dominate in May–September. The lack of fire-driven trends is likely due both to long time averaging and large uncertainties HCHO retrievals under fire conditions.

Decreasing NO_x emissions might also be expected to drive trends in HCHO. Oxidation of VOCs produces organic peroxy radicals that can either react with NO (high-NO_x pathway) or undergo isomerization or reaction with the hydroperoxy radical (low-NO_x pathways). The high-NO_x pathway has a higher HCHO yield [*Marais et al.*, 2012; *Wolfe et al.*, 2016; *Chan Miller et al.*, 2016]. In response to air quality regulations, anthropogenic NO_x emissions in the U.S. have decreased by $4.5\%\ a^{-1}$ over 2005–2014 (https://www.epa.gov/air-emissions-inventories/air-pollutant-emissions-trends-data). In the southeastern U.S., high- and low-NO_x pathways are now of comparable importance for isoprene oxidation [*Travis et al.*, 2016].

To study the impact of decreasing NO_x emissions on HCHO columns, we use the Goddard Earth Observing System (GEOS)-Chem chemical transport model (v10-01; http://geos-chem.org) driven by GEOS-5 assimilated meteorological fields [*Molod et al.*, 2012]. Previous studies by *Zhu et al.* [2016] and *Chan Miller et al.* [2016] indicate that GEOS-Chem is unbiased in reproducing HCHO aircraft observations over the southeastern U.S. We conducted two GEOS-Chem simulations: (1) a control simulation for May–September 2007, representative of the 2005–2009 period, and (2) a sensitivity simulation the same as the control but with a 20% reduction of U.S. anthropogenic NO_x emissions, representative of the 2010–2014 period. Other model configurations are the same as in *Zhu et al.* [2017]. As expected, HCHO columns generally decline by $0.1–0.7 \times 10^{15}$ molecules cm^{-2} across North America in the sensitivity simulation (not shown). The mean decrease is 0.2×10^{15} molecules cm^{-2} over the southeastern U.S., accounting for ~20% of the mean change seen by OMI (Figure 1). Over some urban areas with high NO_x emissions, however, HCHO columns increase slightly by $0.1–0.2 \times 10^{15}$ molecules cm^{-2} in the sensitivity simulation, likely due to the increase in OH as NO_x emissions decrease under NO_x-saturated conditions. These responses in HCHO column are small relative to

the changes in column amount seen by OMI (Figure 1). *Travis et al.* [2016] found that the branching ratio between high-NO_x and low-NO_x pathways for isoprene oxidation responds only weakly to changes in anthropogenic NO_x emissions because of the spatial segregation of NO_x and isoprene emissions.

In conclusion, we have used OMI satellite observations to diagnose long-term trends in HCHO columns across North America from 2005 to 2014. Controlled for temperature, HCHO generally increased from 2005–2009 to 2010–2014 but decreased in the southeastern U.S. We find significant regional trends in excess of 20% related to decreases in urban anthropogenic VOC emissions (Houston metropolitan area) and increases in oil/gas production (southern Alberta in Canada). Significant regional variability in the northwestern U.S. and in the Midwest may be driven by afforestation and agricultural activity. The impact of declining NO_x emission over the U.S. on HCHO columns is likely small over this time frame.

Acknowledgments
This work was funded by the NASA Earth Science Division as part of the Aura Science Team. OMI HCHO data were obtained freely from the NASA Goddard Earth Sciences Data and Information Services Center (https://disc.gsfc.nasa.gov/Aura/data-holdings/OMI/omhcho_v003.shtml). MERRA-2 surface skin temperature data were generated by the NASA Global Modeling and Assimilation Office (https://gmao.gsfc.nasa.gov/reanalysis/MERRA/).

References

Abbot, D. S., P. I. Palmer, R. V. Martin, K. V. Chance, D. J. Jacob, and A. Guenther (2003), Seasonal and interannual variability of North American isoprene emissions as determined by formaldehyde column measurements from space, *Geophys. Res. Lett.*, *30*(17), 1886, doi:10.1029/2003GL017336.

Anderson, D., J. Nicely, R. Salawitch, G. Wolfe, T. Hanisco, R. Dickerson, T. Canty, and C. Li (2016), Evaluation of satellite HCHO retrievals over the tropical western Pacific and United States, Abstract presented at 2016 Fall Meeting, AGU, San Francisco, Calif., 3–7 Dec.

Alvarado, M. J., et al. (2015), Investigating the links between ozone and organic aerosol chemistry in a biomass burning plume from a prescribed fire in California chaparral, *Atmos. Chem. Phys.*, *15*, 6667–6688, doi:10.5194/acp-15-6667-2015.

Amosa, M.K., I.A. Mohammed, and S.A. Yaro (2010), Sulphide scavengers in oil and gas industry—A review, *NAFTA*, *61*(2), 85–92.

Barkley, M. P., et al. (2013), Top-down isoprene emissions over tropical South America inferred from SCIAMACHY and OMI formaldehyde columns, *J. Geophys. Res. Atmos.*, *118*, 6849–6868, doi:10.1002/jgrd.50552.

Bauwens, M., T. Stavrakou, J.-F. Müller, I. De Smedt, M. Van Roozendael, G. R. van der Werf, C. Wiedinmyer, J. W. Kaiser, K. Sindelarova, and A. Guenther (2016), Nine years of global hydrocarbon emissions based on source inversion of OMI formaldehyde observations, *Atmos. Chem. Phys.*, *16*, 10,133–10,158, doi:10.5194/acp-16-10133-2016.

Boeke, N. L., et al. (2011), Formaldehyde columns from the Ozone Monitoring Instrument: Urban versus background levels and evaluation using aircraft data and a global model, *J. Geophys. Res.*, *116*, D05303, doi:10.1029/2010JD014870.

Chance, K., P. I. Palmer, R. J. D. Spurr, R. V. Martin, T. P. Kurosu, and D. J. Jacob (2000), Satellite observations of formaldehyde over North America from GOME, *Geophys. Res. Lett.*, *27*, 3461–3464, doi:10.1029/2000GL011857.

Chan Miller, C., et al. (2016), Glyoxal yield from isoprene oxidation and relation to formaldehyde: Chemical mechanism, constraints from SENEX aircraft observations, and interpretation of OMI satellite data, *Atmos. Chem. Phys. Discuss.*, doi:10.5194/acp-2016-1042.

Cornbleet, P.J., and N. Gochman (1979), Incorrect least-squares regression coefficients in method-comparison analysis, *Clin. Chem.*, *25*, 432–438.

de Gouw, J. A., et al. (2015), Airborne measurements of the atmospheric emissions from a fuel ethanol refinery, *J. Geophys. Res. Atmos.*, *120*, 4385–4397, doi:10.1002/2015JD023138.

de Graaf, M., H. Sihler, L. G. Tilstra, and P. Stammes (2016), How big is an OMI pixel?, *Atmos. Meas. Tech.*, *9*, 3607–3618, doi:10.5194/amt-9-3607-2016.

De Smedt, I., J.-F. Müller, T. Stavrakou, R. van der A, H. Eskes, and M. Van Roozendael (2008), Twelve years of global observations of formaldehyde in the troposphere using GOME and SCIAMACHY sensors, *Atmos. Chem. Phys.*, *8*, 4947–4963, doi:10.5194/acp-8-4947-2008.

De Smedt, I., T. Stavrakou, J.-F. Müller, R. J. van der Abo, and M. Van Roozendael (2010), Trend detection in satellite observations of formaldehyde tropospheric columns, *Geophys. Res. Lett.*, *37*, L18808, doi:10.1029/2010GL044245.

De Smedt, I., et al. (2015), Diurnal, seasonal and long-term variations of global formaldehyde columns inferred from combined OMI and GOME-2 observations, *Atmos. Chem. Phys.*, *15*, 12,519–12,545, doi:10.5194/acp-15-12519-2015.

Duncan, B. N., Y. Yoshida, M. R. Damon, A. R. Douglass, and J. C. Witte (2009), Temperature dependence of factors controlling isoprene emissions, *Geophys. Res. Lett.*, *36*, L05813, doi:10.1029/2008GL037090.

Edwards, P. M., et al. (2014), High winter ozone pollution from carbonyl photolysis in an oil and gas basin, *Nature*, *514*, 351–354, doi:10.1038/nature13767.

ETS (Energy Technical Services) (2016), *Oil Sands Production Profile: 2004–2014*, pp. 1–24, Alberta Energy, Edmonton, Alberta, Canada. [Available at http://www.energy.alberta.ca/Org/pdfs/InitiativeOSPP.pdf.]

Friedl, M. A., D. Sulla-Menashe, B. Tan, A. Schneider, N. Ramankutty, A. Sibley, and X. Huang (2010), MODIS Collection 5 global land cover: Algorithm refinements and characterization of new datasets, *Remote Sens. Environ.*, *114*, 168–182.

Fu, T.-M., D. J. Jacob, P. I. Palmer, K. Chance, Y. X. Wang, B. Barletta, D. R. Blake, J. C. Stanton, and M. J. Pilling (2007), Space-based formaldehyde measurements as constraints on volatile organic compound emissions in east and south Asia and implications for ozone, *J. Geophys. Res.*, *112*, D06312, doi:10.1029/2006JD007853.

Gilman, J. B., et al. (2009), Measurements of volatile organic compounds during the 2006 TexAQS/GoMACCS campaign: Industrial influences, regional characteristics, and diurnal dependencies of the OH reactivity, *J. Geophys. Res.*, *114*, D00F06, doi:10.1029/2008JD011525.

Gilman, J. B., B. M. Lerner, W. C. Kuster, and J. A. de Gouw (2013), Source signature of volatile organic compounds from oil and natural gas operations in northeastern Colorado, *Environ. Sci. Technol.*, *47*(3), 1297–305, doi:10.1021/es304119a.

González Abad, G., X. Liu, C. Chance, A. Fried, and H. Irie (2014), Validation of the new SAO OMI formaldehyde retrievals, Abstract presented at 2014 Fall Meeting, AGU, San Francisco, Calif., 15–19 Dec.

González Abad, G., X. Liu, K. Chance, H. Wang, T. P. Kurosu, and R. Suleiman (2015), Updated Smithsonian Astrophysical Observatory Ozone Monitoring Instrument (SAO OMI) formaldehyde retrieval, *Atmos. Meas. Tech.*, *8*, 19–32, doi:10.5194/amt-8-19-2015.

Gonzi, S., P. I. Palmer, M. P. Barkley, I. De Smedt, and M. Van Roozendael (2011), Biomass burning emission estimates inferred from satellite column measurements of HCHO: Sensitivity to co-emitted aerosol and injection height, *Geophys. Res. Lett.*, *38*, L14807, doi:10.1029/2011GL047890.

Guenther, A., T. Karl, P. Harley, C. Wiedinmyer, P. I. Palmer, and C. Geron (2006), Estimates of global terrestrial isoprene emissions using MEGAN (Model of Emissions of Gases and Aerosols from Nature), *Atmos. Chem. Phys.*, *6*, 3181–3210, doi:10.5194/acp-6-3181-2006.

Guenther, A. B., X. Jiang, C. L. Heald, T. Sakulyanontvittaya, T. Duhl, L. K. Emmons, and X. Wang (2012), The Model of Emissions of Gases and Aerosols from Nature version 2.1 (MEGAN2.1): An extended and updated framework for modeling biogenic emissions, *Geosci. Model Dev.*, *5*, 1471–1492, doi:10.5194/gmd-5-1471-2012.

Hafner, S. D., C. Howard, R. E. Muck, R. B. Franco, F. Montes, P. G. Green, F. Mitloehner, S. L. Trabue, and C. A. Rotz (2013), Emission of volatile organic compounds from silage: Compounds, sources, and implications, *Atmos. Environ.*, *77*, 827–839.

Hansen, M. C., et al. (2013), High-resolution global maps of 21st-century forest cover change, *Science*, *342*, 850–853, doi:10.1126/science.1244693.

Kaiser, J., et al. (2015), Evidence for an unidentified non-photochemical ground-level source of formaldehyde in the Po Valley with potential implications for ozone production, *Atmos. Chem. Phys.*, *15*, 1289–1298, doi:10.5194/acp-15-1289-2015.

Kenreck, G. (2014), Manage hydrogen sulfide hazards with chemical scavengers, *Hydrocarbon Process.*, 73–76. [Avaialbe at https://www.gewater.com/kcpguest/documents/Technical Papers_Cust/Americas/English/HP_Dec2014_Manage_Hydrogen_Sulfide_Hazards_with_Chemical_Scavengers.pdf.]

Khokhar, M., C. Frankenberg, M. V. Roozendael, S. Beirle, S Kuhl, A. Richter, U. Platt, and T. Wagner (2005), Satellite observations of atmospheric SO_2 from volcanic eruptions during the time-period of 1996–2002, *Adv. Space Res.*, *36*, 879–887.

Levelt, P. F., G. H. J. van den Oord, M. R. Dobber, A. Malkki, H. Visser, J. de Vries, P. Stammes, J. O. V. Lundell, and H. Saari (2006), The Ozone Monitoring Instrument, *IEEE Trans. Geophys. Remote Sens.*, *44*, 1093–1101.

Macey, G. P., R. Breech, M. Chernaik, C. Cox, D. Larson, D. Thomas, and D. O. Carpenter (2014), Air concentrations of volatile compounds near oil and gas production: A community-based exploratory study, *Environ. Health*, *13*, 82, doi:10.1186/1476-069X-13-82.

Marais, E. A., et al. (2012), Isoprene emissions in Africa inferred from OMI observations of formaldehyde columns, *Atmos. Chem. Phys.*, *12*, 6219–6235, doi:10.5194/acp-12-6219-2012.

Marais, E. A., D. J. Jacob, K. Wecht, C. Lerot, L. Zhang, K. Yu, T. P. Kurosu, K. Chance, and B. Sauvage (2014), Anthropogenic emissions in Nigeria and implications for ozone air quality: A view from space, *Atmos. Environ.*, *99*, 32–40, doi:10.1016/j.atmosenv.2014.09.055.

McLinden, C. A., V. Fioletov, K. F. Boersma, N. Krotkov, C. E. Sioris, J. P. Veefkind, and K. Yang (2012), Air quality over the Canadian oil sands: A first assessment using satellite observations, *Geophys. Res. Lett.*, *39*, L04804, doi:10.1029/2011GL050273.

Millet, D. B., et al. (2006), Formaldehyde distribution over North America: Implications for satellite retrievals of formaldehyde columns and isoprene emission, *J. Geophys. Res.*, *111*, D24S02, doi:10.1029/2005JD006853.

Millet, D. B., D. J. Jacob, K. F. Boersma, T. M. Fu, T. P. Kurosu, K. Chance, C. L. Heald, and A. Guenther (2008), Spatial distribution of isoprene emissions from North America derived from formaldehyde column measurements by the OMI satellite sensor, *J. Geophys. Res.*, *113*, D02307, doi:10.1029/2007JD008950.

Molod, A., L. Takacs, M. Suarez, J. Bacmeister, I.-S. Song, and A. Eichmann (2012), The GEOS-5 Atmospheric General Circulation Model: Mean Climate and Development from MERRA to Fortuna, *NASA/TM–2012*, *104606*, 28, 1–124.

Palmer, P. I., D. J. Jacob, A. M. Fiore, R. V. Martin, K. Chance, and T. P. Kurosu (2003), Mapping isoprene emissions over North America using formaldehyde column observations from space, *J. Geophys. Res.*, *108*(D6), 4180, doi:10.1029/2002JD002153.

Palmer, P. I., et al. (2006), Quantifying the seasonal and interannual variability of North American isoprene emissions using satellite observations of the formaldehyde column, *J. Geophys. Res.*, *111*, D12315, doi:10.1029/2005JD006689.

Pikelnaya, O., J. H. Flynn, C. Tsai, and J. Stutz (2013), Imaging DOAS detection of primary formaldehyde and sulfur dioxide emissions from petrochemical flares, *J. Geophys. Res. Atmos.*, *118*, 8716–8728, doi:10.1002/jgrd.50643.

Shim, C., Y. Wang, Y. Choi, P. I. Palmer, D. S. Abbot, and K. Chance (2005), Constraining global isoprene emissions with Global Ozone Monitoring Experiment (GOME) formaldehyde column measurements, *J. Geophys. Res.*, *110*, D24301, doi:10.1029/2004JD005629.

Souri, A. H., Y. Choi, W. Jeon, J.-H. Woo, Q. Zhang, and J.-i. Kurokawa (2017), Remote sensing evidence of decadal changes in major tropospheric ozone precursors over East Asia, *J. Geophys. Res. Atmos.*, *122*, 2474–2492, doi:10.1002/2016JD025663.

Stavrakou, T., J.-F. Müller, I. De Smedt, M. Van Roozendael, G. R. van der Werf, L. Giglio, and A. Guenther (2009), Global emissions of non-methane hydrocarbons deduced from SCIAMACHY formaldehyde columns through 2003–2006, *Atmos. Chem. Phys.*, *9*, 3663–3679, doi:10.5194/acp-9-3663-2009.

Toon, O. B., et al. (2016), Planning, implementation, and scientific goals of the Studies of Emissions and Atmospheric Composition, Clouds and Climate Coupling by Regional Surveys ($SEAC^4RS$) field mission, *J. Geophys. Res. Atmos.*, *121*, 4967–5009, doi:10.1002/2015JD024297.

Travis, K. R., et al. (2016), Why do models overestimate surface ozone in the Southeast United States?, *Atmos. Chem. Phys.*, *16*, 13,561–13,577, doi:10.5194/acp-16-13561-2016.

Wolfe, G. M., et al. (2016), Formaldehyde production from isoprene oxidation across NO_x regimes, *Atmos. Chem. Phys.*, *16*, 2597–2610, doi:10.5194/acp-16-2597-2016.

Zhu, L., D. J. Jacob, L. J. Mickley, E. A. Marais, D. S. Cohan, Y. Yoshida, B. N. Duncan, G. González Abad, and K. V. Chance (2014), Anthropogenic emissions of highly reactive volatile organic compounds in eastern Texas inferred from oversampling of satellite (OMI) measurements of HCHO columns, *Environ. Res. Lett.*, *9*, 114004, doi:10.1088/1748-9326/9/11/114004.

Zhu, L., et al. (2016), Observing atmospheric formaldehyde (HCHO) from space: Validation and intercomparison of six retrievals from four satellites (OMI, GOME2A, GOME2B, OMPS) with $SEAC^4RS$ aircraft observations over the southeast US, *Atmos. Chem. Phys.*, *16*, 13,477–134,90, doi:10.5194/acp-16-13477-2016.

Zhu, L., et al. (2017), Formaldehyde (HCHO) as a hazardous air pollutant: Mapping surface air concentrations from satellite and inferring cancer risks in the United States, *Environ. Sci. Technol.*, *51*, 5650–5657, doi:10.1021/acs.est.7b01356.